1-18-2013

Subdiffraction, Luminescence-Depletion Imaging of Isolated, Giant, CdSe/CdS Nanocrystal Quantum Dots

Michael D. Lesoine
Iowa State University

Ujjal Bhattacharjee
Iowa State University, ujjalb@iastate.edu

Yijun Guo
Iowa State University

Javier Vela-Becerra
Iowa State University, vela@iastate.edu

Jacob W. Petrich
Iowa State University, jwp@iastate.edu

See next page for additional authors

Subdiffraction, Luminescence-Depletion Imaging of Isolated, Giant, CdSe/CdS Nanocrystal Quantum Dots

Abstract

Subdiffraction spatial resolution luminescence depletion imaging was performed with giant CdSe/14CdS nanocrystal quantum dots (g-NQDs) dispersed on a glass slide. Luminescence depletion imaging used a Gaussian shaped excitation laser pulse overlapped with a depletion pulse, shaped into a doughnut profile, with zero intensity in the center. Luminescence from a subdiffraction volume is collected from the central portion of the excitation spot, where no depletion takes place. Up to 92% depletion of the luminescence signal was achieved. An average full width at half-maximum of 40 ± 10 nm was measured in the lateral direction for isolated g-NQDs at an air interface using luminescence depletion imaging, whereas the average full width at half-maximum was 450 ± 90 nm using diffraction-limited, confocal luminescence imaging. Time-gating of the luminescence depletion data was required to achieve the stated spatial resolution. No observable photobleaching of the g-NQDs was present in the measurements, which allowed imaging with a dwell time of 250 ms per pixel to obtain images with a high signal-to-noise ratio. The mechanism for luminescence depletion is likely stimulated emission, stimulated absorption, or a combination of the two. The g-NQDs fulfill a need for versatile, photostable tags for subdiffraction imaging schemes where high laser powers or long exposure times are used.

Disciplines

Chemistry | Environmental Chemistry | Materials Chemistry | Organic Chemistry | Other Chemistry | Physical Chemistry

Comments

Reprinted (adapted) with permission from *The Journal of Physical Chemistry C,* 117(7); 3662-3667. Doi: 10.1021/jp312231k.

Authors

Michael D. Lesoine, Ujjal Bhattacharjee, Yijun Guo, Javier Vela-Becerra, Jacob W. Petrich, and Emily A. Smith

THE JOURNAL OF PHYSICAL CHEMISTRY C

Article

pubs.acs.org/JPCC

Subdiffraction, Luminescence-Depletion Imaging of Isolated, Giant, CdSe/CdS Nanocrystal Quantum Dots

Michael D. Lesoine,[†,‡] Ujjal Bhattacharjee,[†,‡] Yijun Guo,[†,‡] Javier Vela,[†,‡] Jacob W. Petrich,*[,†,‡] and Emily A. Smith*[,†,‡]

[†]U.S. Department of Energy, Ames Laboratory, Ames, Iowa 50011, United States

[‡]Department of Chemistry, Iowa State University, 1605 Gilman Hall, Ames, Iowa 50011, United States

ABSTRACT: Subdiffraction spatial resolution luminescence depletion imaging was performed with giant CdSe/14CdS nanocrystal quantum dots (g-NQDs) dispersed on a glass slide. Luminescence depletion imaging used a Gaussian shaped excitation laser pulse overlapped with a depletion pulse, shaped into a doughnut profile, with zero intensity in the center. Luminescence from a subdiffraction volume is collected from the central portion of the excitation spot, where no depletion takes place. Up to 92% depletion of the luminescence signal was achieved. An average full width at half-maximum of 40 ± 10 nm was measured in the lateral direction for isolated g-NQDs at an air interface using luminescence depletion imaging, whereas the average full width at half-maximum was 450 ± 90 nm using diffraction-limited, confocal luminescence imaging. Time-gating of the luminescence depletion data was required to achieve the stated spatial resolution. No observable photobleaching of the g-NQDs was present in the measurements, which allowed imaging with a dwell time of 250 ms per pixel to obtain images with a high signal-to-noise ratio. The mechanism for luminescence depletion is likely stimulated emission, stimulated absorption, or a combination of the two. The g-NQDs fulfill a need for versatile, photostable tags for subdiffraction imaging schemes where high laser powers or long exposure times are used.

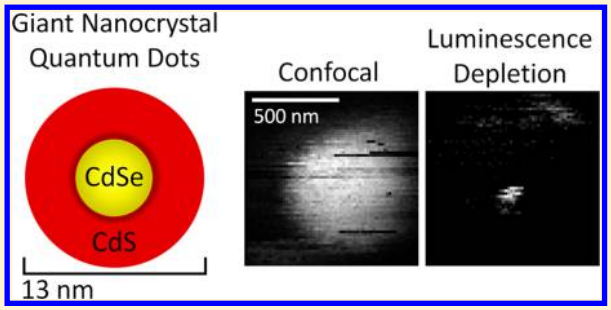

INTRODUCTION

Lateral spatial resolution using visible wavelengths is limited by diffraction to ~250 nm in far-field optical microscopy.[1] There are several imaging techniques available to circumvent this constraint. Near-field techniques with a probe in close proximity to the sample can be used, but the probe can be too invasive for some applications.[2] In addition to using a near-field technique, there are several far-field techniques that have been developed. Stochastic optical reconstruction microscopy and several similar techniques utilize intermittent on/off states to limit the number of fluorophores emitting in a diffraction limited volume, and to generate a series of images that are reconstructed into a high resolution image.[3] Stimulated emission depletion (STED) microscopy uses point-spread function engineering, and can yield measurements with high spatial and temporal resolution.[4−12] STED uses a doughnut shaped depletion beam that spatially and temporally overlaps a Gaussian shaped excitation beam. The depletion beam is tuned to the red edge of a fluorophore's emission spectrum, providing depletion of the signal at the periphery of the Gaussian excitation profile. The resulting signal from the center of the excitation profile is below the diffraction limit.

In order to achieve subdiffraction spatial resolution imaging with STED, high laser powers or long acquisition times may be required. These conditions may lead to significant photobleaching of most small molecule fluorophores, which can degrade the achieved spatial resolution.[13,14] Nanocrystal quantum dots (NQDs) display the highest photostability of the prominently used fluorescent labels,[15,16] making them an ideal fluorophore for STED. On the other hand, Auger recombination, for example, is known to prevent efficient stimulated emission of isolated NQDs.[17] Stimulated emission can outpace Auger recombination in close-packed solids and highly concentrated colloidal solutions,[18,19] but extended solids have limited utility as tags for imaging applications.

Hell and co-workers demonstrated 45 nm spatial resolution along a single axis for clusters of Mn-doped ZnSe NQDs using a depletion beam with two nodes having zero intensity between them.[20] They attributed the improved spatial resolution to stimulated absorption to higher-lying excited states.[21] Clusters of NQDs were necessary for their study to avoid excessive exposure times, as sufficient signal could not be obtained with isolated NQDs due to a long lifetime (about 90 μs) of the luminescence transition.

So-called giant NQDs (g-NQDs) with 10−20 monolayers of CdS shell added onto a 2−5 nm CdSe core exhibit suppression of luminescence intermittency (i.e., blinking) and almost complete suppression of Auger recombination.[22−25] The suppression of Auger recombination has the effect of increasing the lifetime of biexcitons and even allowing the observation of

Received: December 12, 2012
Revised: January 14, 2013
Published: January 18, 2013

   dx.doi.org/10.1021/jp312231k | J. Phys. Chem. C 2013, 117, 3662−3667

multiexciton states.[26] Radiative lifetime components of excitons, biexcitons, and up to sixth-order multiexcitons in g-NQDs were observed with excitation powers on the order of 1 kW cm^{-2} at 4 K.[26] Furthermore, biexcitons and multiexcitons can undergo more effective stimulated emission, with the multiexcitons having a lower threshold for stimulated emission than biexcitons and indeed many dye molecules.[23]

Here, we report luminescence depletion (LD) imaging using CdSe/14CdS g-NQDs with a lateral spatial resolution of 40 ± 10 nm. It is proposed that stimulated emission and excited-state absorption mechanisms may work either independently or synergistically to provide depletion. A 7-fold improvement over the diffraction barrier was generated at an air interface with excitation and depletion powers of 50 pJ and 2 nJ, respectively.

EXPERIMENTAL SECTION

Sample Preparation and Characterization. The g-NQDs have been previously described.[27] The average CdSe/14CdS g-NQD particle size was 13 ± 2 nm as measured by transmission electron microscopy. Single particle films used in imaging experiments were prepared by depositing isolated giant CdSe/14CdS quantum dots by a method demonstrated previously.[22,24] Briefly, giant CdSe/14CdS quantum dots were diluted in toluene to a concentration in the ca. 0.1−50 pM range. Solutions were sonicated and deposited on a glass slide (474030-9000-000, Carl Zeiss Microscopy, Thornwood, NY), and the solvent was allowed to evaporate. We previously demonstrated that samples prepared in this way showed no sign of aggregation before or after making the films. This conclusion was based on several measurements, including antibunching experiments.[28] The sample was dried under ambient conditions for 30 min before any measurements were performed.

Blinking statistics for the g-NQDs were determined by comparing the percent of time the signal was in a binary high (on) or low (off) state using sequential 25 ms measurements over a 95 s time window. Depletion efficiencies for the g-NQDs were measured as the attenuation of the luminescence signal after illumination with the excitation and depletion wavelengths compared to the signal with illumination of only the excitation wavelength. The depletion power was varied, and sequential 250 ms measurements over a 45 s time window were collected. Depletion was also observed with a CMOS camera (Moticam 2, Motic, British Columbia, Canada) by illuminating a single NQD with the excitation beam and blocking and unblocking the LD beam. Photobleaching rates for the g-NQDs were measured by illuminating the samples with the excitation beam at the same position and taking sequential time measurements over 3.5 min. For all measurements described above, the beams had a Gaussian profile.

Imaging. The imaging system used for these studies has been described previously.[29] Minor changes to the system are described below. The excitation and depletion beams derive from an SC laser (SC-450-pp-he, Fianium, Southampton, U.K.), which has its output split into two paths using a polarizing beam splitter cube (DMLP605R, Thorlabs, Newton, New Jersey). The laser repetition rate was 2 MHz, and the pulse widths for the excitation and LD pulses were approximately 120 and 160 ps, respectively. The two pulses were offset with the LD pulse trailing the excitation pulse by ~100 ps. Filters are used to select the excitation and LD wavelengths, which are shown in Figure 1. Measurements were performed using 50 pJ for excitation and 2 nJ for LD, as measured before the microscope objective. The excitation and

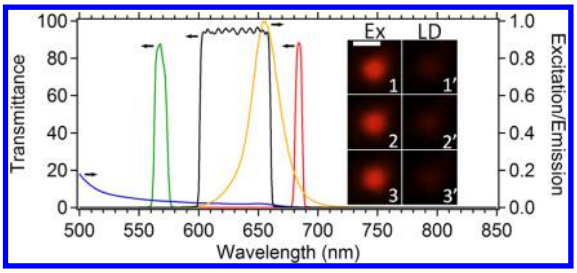

Figure 1. The CdSe/14CdS g-NQD excitation (blue line) and emission (orange line) spectra and the transmission curves for the microscope's filters are shown. The laser pulses are selected with interference filters with the excitation (green line) and LD (red line) filters centered at 570 ± 10 and 684 ± 8 nm, respectively. The band-pass of the LD filter allows significant overlap with the g-NQD emission spectrum while avoiding unwanted excitation. Two stacked emission filters (black line) centered at 630 ± 60 nm allow the signal to be transmitted to the detection path. The inset shows the NQDs LD is reversible with successive images from top to bottom of a single quantum dot obtained with excitation beam illumination (left column) or excitation plus depletion beam illumination (right column), where all beams were Gaussian shaped. The scale bar is 500 nm.

LD pulses were ~350 and ~600 nm (with a center null) in diameter at the focal plane, respectively. The LD beam was shaped into a doughnut with a vortex-phase plate. The beams are expanded and collimated before being recombined using a dichroic mirror (ZT594RDC, Chroma, Bellows Falls, Vermont). The collinear pulses are reflected via a dichroic mirror (635-70BPDC, Chroma) to an oil immersion objective, and the resulting luminescence is directed to the detection path. The signal is sent to two stacked emission filters (FF01-629/56-25, Semrock, Rochester, NY) and subsequently through a 100 μm pinhole (NT36-392, Edmund Optics, Barrington, NJ) and a hybrid photomultiplier tube (HPM-100-40, Becker and Hickl, Berlin, Germany) coupled to a single-photon counting card (SPC-830, Becker and Hickl).

Raster scanning of a 1 × 1 μm (64 × 64 pixels) or 2 × 2 μm (128 × 128 pixels) region was used to generate the images. Images were collected at room temperature. All data were collected with Single Photon Counter v9.30 software (Becker & Hickl) and analyzed further using SPCImage (Becker & Hickl) or MATLAB version 2011b (Mathworks, Natick, MA). A time window of 3.3 ns with 64 time channels and a dwell time of 250 ms per pixel were used. Time-gating was used to obtain the best spatial resolution, as further outlined below. Image-J 1.44p (National Institutes of Health, USA) was used to take cross sections of contiguous pixels in the collected images, and Origin (OriginLab, Northampton, MA) was used to perform all other data processing. All reported uncertainties are one standard deviation.

RESULTS AND DISCUSSION

Luminescence Depletion Efficiencies of g-NQDs. The goal of this work was to explore the ability of giant nanocrystal quantum dots (g-NQDs) to serve as photostable tags for subdiffraction imaging techniques that require high laser powers and/or long exposure times. In practice, this required determining the experimental conditions, including laser powers, acquisition times, and signal gating, necessary for subdiffraction imaging using g-NQDs. As observed in Figure 1, the g-NQDs display the characteristic broad excitation curve (blue curve). The excitation wavelengths (green curve) were

dx.doi.org/10.1021/jp312231k | J. Phys. Chem. C 2013, 117, 3662−3667

chosen to be as far red-shifted as possible in order to limit scattering, photodamage, and background luminescence in future applications where this may be an issue, such as in the case of biological samples, without compromising the desired signal collection. The amount of spectral overlap between the g-NQD's narrow emission profile (orange curve) and the depletion wavelengths (red curve) had to be carefully balanced. A too small overlap would lead to inefficient depletion, while an unnecessarily large overlap would cause an unwanted decrease in signal collection from a narrow detection window (black curve). LD occurs with the chosen excitation and depletion wavelengths (Figure 1, inset). In this instance, both the excitation and depletion beams were Gaussian shaped, and the data reveal that the depletion is reversible.

The optimum power of the depletion beam results in 100% LD efficiency without excessive exposure of the sample to high photon fluxes, thus limiting sample heating and damage. In order to determine the optimal power for the depletion beam, the attenuation of the luminescence signal for isolated g-NQDs was recorded for varying depletion powers (Figure 2). The

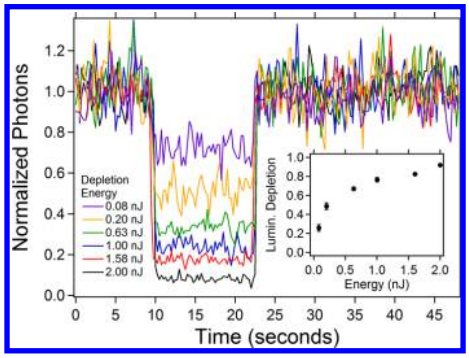

Figure 2. The g-NQD depletion efficiency was measured using continuous illumination with the 50 pJ excitation beam, and overlapping the depletion beam after approximately 10 s had elapsed. The depletion energies ranged from 0.08 to 2.00 nJ. The data were corrected for a small component of luminescence generated by the depletion beam but did not need correction for photobleaching. The inset shows the fraction of LD versus depletion laser energy.

depletion efficiency increases with increasing depletion power up to the maximum output of the laser used for these studies (2.0 nJ). At the highest power, a 92% depletion was obtained after correcting for a 3% contribution to the luminescence signal caused by the depletion beam. The mechanism of the high depletion efficiency could be stimulated emission, stimulated absorption, or both. Stimulated absorption has been shown for Mn-doped ZnSe NQDs.[20] A definitive assignment of the mechanism will, however, require further experiments that are beyond the scope of this work.

Determination of g-NQD On/Off Time and Photobleaching Rates. A zero or low frequency of blinking events is desirable for raster scan imaging to maintain the generated image's integrity. For an imaging application, a dwell time that is too short relative to the blinking characteristics of the nanoparticle will result in an undesired false negative at that pixel; on the other hand, it is not desirable to ensure there are no false negatives, as excessive imaging times may result. The blinking characteristics of the g-NQDs must be known to set a dwell time per pixel that limits false negatives and to quantify the probability of recording a false negative at an acceptable imaging speed. Therefore, the luminescence signal of isolated g-NQDs was recorded over a time window of 95 s using an excitation power of 50 pJ. Representative data from 10 randomly chosen g-NQDs are shown in Figure 3. The average

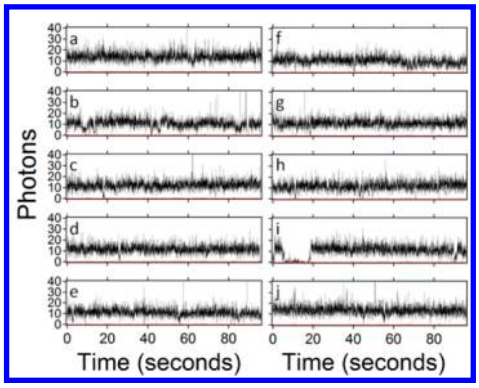

Figure 3. Graphs of the luminescence intensity versus time for 10 individual g-NQDs labeled a–j. The luminescence intensity was integrated every 25 ms for a total of 95 s. The excitation power was the same as used for collecting the LD images (50 pJ). The NQD was considered off if the signal dropped below 3 counts for 3 adjacent data points. The data show g-NQDs under the experimental conditions used here were 90% nonblinking with on-times greater than 99% and 10% largely nonblinking with on-times between 99 and 80%.

percent on-time for all nanoparticles was 98.40 ± 0.04%. Hollingsworth and co-workers reported an on-time of greater than 99% and between 99 and 80% of the total analysis time as corresponding to nonblinking and largely nonblinking g-NQDs, respectively.[24] The percentage of particles with on-times greater than 99% was 90%, and the average off-time for these particles was 100 ± 200 ms. The percentage of particles with on-times between 99 and 80% was 10%. The observed nonblinking behavior is typical of isolated giant CdSe/nCdS quantum dots.[24,27,30]

No observable photobleaching was observed on the time-scale of any of the measurements performed, which included an extended 3.5 min illumination of the g-NQDs. This allowed for dwell times per pixel not possible with typical fluorescent dyes used for STED, including the 250 ms dwell time used for subsequent experiments.

Subdiffraction Spatial Resolution Imaging Using g-NQDs. The confocal and LD images of 12 quantum dots are shown in Figure 4. The confocal images were recorded using only the excitation beam, while both the excitation and depletion beams were incident upon the sample for the LD images. The improvement in the spatial resolution of the LD images is evident by the smaller feature size. In the confocal images, there are occasional rows of lower luminescence intensity compared to the rest of the pixels representing the g-NQD. This is attributed to a few intermittent blinking periods, characteristic of even the best g-NQDs. The amount of intermittent blinking recorded in the LD images is significantly lower than that in the confocal images, and is only observed for g-NQD number 6. This is expected, since the total time used to collect the nanoparticle's luminescence signal (not the time the nanoparticle is exposed to the laser) in the LD mode is 97.7 ± 0.8% shorter than that used to collect the confocal image.

Cross sections were measured for each g-NQD shown in Figure 4, and representative cross sections are shown in Figure 5. The confocal cross sections were best fit to Gaussians, while the LD cross sections were best fit to Lorentzians. This is

dx.doi.org/10.1021/jp312231k | J. Phys. Chem. C 2013, 117, 3662–3667

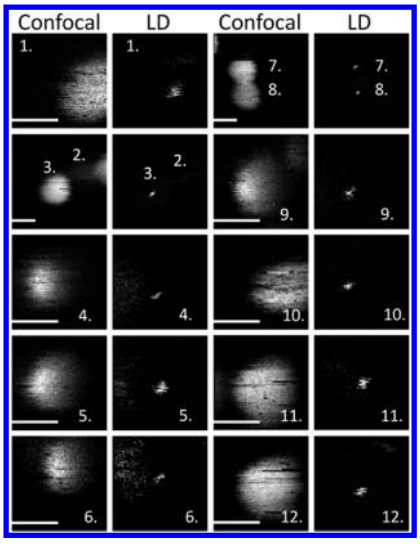

Figure 4. Images of 12 g-NQDs measured in the confocal and LD modes. The confocal images were collected after blocking the depletion beam, and the doughnut shaped depletion beam was unblocked to generate the LD images. The scan direction was from left to right and back right to left with a stage step size of 15.6 nm. A stage repeatability of tens of nanometers results in a small shift from the confocal to LD image. Scale bars are all equal to 500 nm.

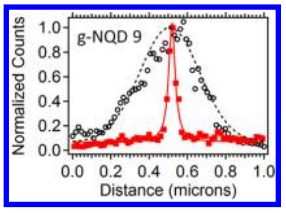

Figure 5. Representative cross sections and associated fits for a g-NQD in confocal (open black circles, Gaussian fit with 398 fwhm) and time-gated LD (solid red squares, Lorentzian fit with 43 nm fwhm) modes. The time-gate applied to the LD images yields an improvement of 2.25 fold over the ungated LD data. A 7× average lateral resolution improvement is observed for the time-gated STED data over the system's diffraction limit.

consistent with previously reported STED data using small molecule fluorophores.[8,29,31] The representative cross sections in Figure 5 show a resolution enhancement, as defined by the full width at half-maximum (fwhm), from 398 nm for the confocal mode to 43 nm for the LD mode. The average fwhm values for 12 g-NQDs are given in Table 1. The average cross section is 450 ± 90 and 40 ± 10 nm for the confocal and LD modes, respectively. For comparison, the actual "physical" average particle size measured by transmission electron microscopy is 13 ± 2 nm.

In order to achieve the 40 ± 10 nm spatial resolution in the LD imaging mode, we had to time-gate the data. The average fwhm of the LD cross sections prior to applying the time-gate was 90 ± 20 nm. A representative confocal and LD decay curve is shown in Figure 6. The applied time-gate that produced the best spatial resolution is represented by the two vertical lines. The signal prior to 600 ps is higher in the LD curve than the confocal curve. This is likely the result of scatter due to the STED beam, which degrades the spatial resolution. When only the gate at the later times was applied and the entire signal at earlier times was included in the analysis, no improvement in spatial resolution was measured. A time-gate at 500 ps was

Table 1. Full Width at Half-Maximum (fwhm) Values Obtained for Cross Sections of g-NQDs Obtained in the Images Shown in Figure 4

g-NQD number from Figure 4	confocal fwhm (nm)	luminescence depletion (time-gated) fwhm (nm)
1	550	34
2	479	35
3	525	42
4	432	30
5	612	44
6	355	33
7	397	38
8	310	51
9	398	43
10	370	45
11	463	55
12	494	62
average	450 ± 90	40 ± 10

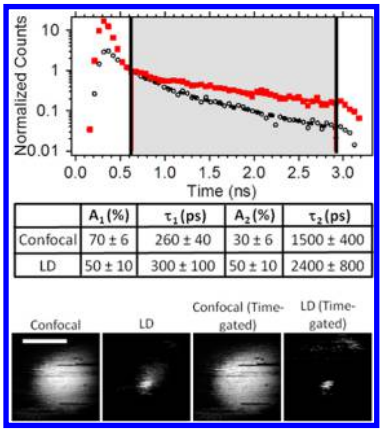

	A_1 (%)	τ_1 (ps)	A_2 (%)	τ_2 (ps)
Confocal	70 ± 6	260 ± 40	30 ± 6	1500 ± 400
LD	50 ± 10	300 ± 100	50 ± 10	2400 ± 800

Figure 6. Top: Representative confocal (open black circles with dotted line fit) and LD (solid red squares with solid line fit) luminescence decay curves are shown at the top of the figure. The vertical lines represent the time-gate that was applied to the LD images in Figure 4. The data have been normalized to the value at 600 ps. Bottom: The two left images show confocal and LD data prior to applying the time-gate, and the two right confocal and LD images show the effects of applying the time-gate. The scale bar is equal to 500 nm.

previously applied to STED images using small molecule fluorophores because depletion was incomplete at earlier times.[29] At long times, the decay curve is primarily dominated by noise that does not convey useful information and degrades the spatial resolution slightly. While gating the signal significantly improved the LD image, gating the confocal data did not significantly alter the average fwhm of the confocal data set (Figure 6, bottom).

Two lifetime components were extracted from the LD data (2400 ± 800 and 300 ± 100 ps). One or both of the lifetime components may originate from multiexcitons. Htoon et al.[26] measured higher-order excitons in similar g-NQDs at 4 K using a 21× lower power density than used in the current study (21 kW cm^{-2} for the excitation beam). The lifetimes of the g-NQDs increase with excitation intensities lower than what was used in the imaging experiments, which is consistent with the g-NQDs existing in multiexcitonic states prior to depletion. The percentage of the short component decreased from 70 ± 6 to 50 ± 10% for the confocal to LD imaging formats, respectively (Figure 6).

dx.doi.org/10.1021/jp312231k | J. Phys. Chem. C 2013, 117, 3662−3667

The overall qualities of the confocal and luminescence decay curves are similar (Figure 6). In a previous experiment using small dye molecules, the noise in the STED decay curve was higher compared to that obtained in the confocal experiment.[29] This was because far fewer molecules were probed by STED, and this reduced the signal. For the small molecule fluorophores, the dwell time per pixel was limited to 5 ms due to excessive photobleaching at longer dwell times. The photostabilty of the g-NQDs allows the dwell time per pixel to be increased, increasing the signal and improving the quality of the decay curve. A 250 ms dwell time was used for these studies, but shorter dwell times could be used to increase the imaging speed, particularly if data are recorded with fewer time channels (i.e., if time-gating is applied but lifetimes are not extracted), while still generating high-quality images with good signal-to-noise ratios.

CONCLUSIONS

Luminescence depletion images of CdSe/14CdS giant nanocrystal quantum dots (g-NQDs) with 13 ± 2 nm particle size have been imaged with 40 ± 10 nm spatial resolution. The mode of resolution enhancement over the diffraction limit is through depletion of the g-NQDs luminescence, suggested to be the result of stimulated emission and absorption working individually or in concert. Time-correlated, single-photon counting detection allowed the signal to be time-gated, which is required for achieving 40 nm spatial resolution. Critical for obtaining this result is that photobleaching was not observed, permitting high quality measurements with extended dwell times that would be difficult to obtain under conditions where photobleaching was present. We conclude that g-NQDs show great promise as robust fluorescent labels for subdiffraction measurements in densely populated systems.

AUTHOR INFORMATION

Corresponding Author

*E-mail: esmith1@iastate.edu (E.A.S.); jwp@iastate.edu (J.W.P.).

Notes

The authors declare no competing financial interest.

ACKNOWLEDGMENTS

This research is supported by the U.S. Department of Energy, Office of Basic Energy Sciences, Division of Chemical Sciences, Geosciences, and Biosciences through the Ames Laboratory. The Ames Laboratory is operated for the U.S. Department of Energy by Iowa State University under Contract No. DE-AC02-07CH11358. The STED microscope was built using funds from the National Science Foundation Chemical Research Instrumentation and Facilities program (CHE-1026028). J.V. thanks Iowa State University and Plant Sciences Institute for seed funds.

REFERENCES

(1) Abbe, E. Beiträge zur Theorie des Mikroskops und der Mikroskopischen Wahrnehmung. *Arch. Mikrosk. Anat.* **1873**, *9*, 413–418.

(2) Binnig, G.; Quate, C. F.; Gerber, C. Atomic Force Microscope. *Phys. Rev. Lett.* **1986**, *56*, 930–933.

(3) Rust, M. J.; Bates, M.; Zhuang, X. Sub-Diffraction-Limit Imaging by Stochastic Optical Reconstruction Microscopy (STORM). *Nat. Methods* **2006**, *3*, 793–796.

(4) Hell, S. W.; Wichmann, J. Breaking the Diffraction Resolution Limit by Stimulated Emission: Stimulated-Emission-Depletion Fluorescence Microscopy. *Opt. Lett.* **1994**, *19*, 780–782.

(5) Klar, T. A.; Hell, S. W. Subdiffraction Resolution in Far-Field Fluorescence Microscopy. *Opt. Lett.* **1999**, *24*, 954–956.

(6) Klar, T. A.; Engel, E.; Hell, S. W. Breaking Abbe's Diffraction Resolution Limit in Fluorescence Microscopy with Stimulated Emission Depletion Beams of Various Shapes. *Phys. Rev. E* **2001**, *64*, 066613.

(7) Bain, A. J.; Marsh, R. J.; Armoogum, D. A.; Mongin, O.; Porrès, L.; Blanchard-Desce, M. Time-Resolved Stimulated Emission Depletion in Two-Photon Excited States. *Biochem. Soc. Trans.* **2003**, *31*, 1047–1051.

(8) Vicidomini, G.; Moneron, G.; Han, K. Y.; Westphal, V.; Ta, H.; Reuss, M.; Engelhardt, J.; Eggeling, C.; Hell, S. W. Sharper Low-Power STED Nanoscopy by Time Gating. *Nat. Methods* **2011**, *8*, 571–573.

(9) Donnert, G.; Keller, J.; Medda, R.; Andrei, M. A.; Rizzoli, S. O.; Lührmann, R.; Jahn, R.; Eggeling, C.; Hell, S. W. Macromolecular-scale Resolution in Biological Fluorescence Microscopy. *Proc. Natl. Acad. Sci. U.S.A.* **2006**, *103*, 11440–11445.

(10) Willig, K. I.; Keller, J.; Bossi, M.; Hell, S. W. STED Microscopy Resolves Nanoparticle Assemblies. *New J. Phys.* **2006**, *8*, 106–106.

(11) Willig, K. I.; Kellner, R. R.; Medda, R.; Hein, B.; Jakobs, S.; Hell, S. W. Nanoscale Resolution in GFP-Based Microscopy. *Nat. Methods* **2006**, *3*, 721–723.

(12) Rittweger, E.; Han, K. Y.; Irvine, S. E.; Eggeling, C.; Hell, S. W. STED Microscopy Reveals Crystal Colour Centres with Nanometric Resolution. *Nat. Photonics* **2009**, *3*, 144–147.

(13) Wildanger, D.; Medda, R.; Kastrup, L.; Hell, S. W. A Compact STED Microscope Providing 3D Nanoscale Resolution. *J. Microsc.* **2009**, *236*, 35–43.

(14) Hotta, J.-i.; Fron, E.; Dedecker, P.; Janssen, K. P. F.; Li, C.; Müllen, K.; Harke, B.; Bückers, J.; Hell, S. W.; Hofkens, J. Spectroscopic Rationale for Efficient Stimulated-Emission Depletion Microscopy Fluorophores. *J. Am. Chem. Soc.* **2010**, *132*, 5021–5023.

(15) Chen, F.; Gerion, D. Fluorescent CdSe/ZnS Nanocrystal–Peptide Conjugates for Long-Term, Nontoxic Imaging and Nuclear Targeting in Living Cells. *Nano Lett.* **2004**, *4*, 1827–1832.

(16) Boldt, K.; Bruns, O. T.; Gaponik, N.; Eychmüller, A. Comparative Examination of the Stability of Semiconductor Quantum Dots in Various Biochemical Buffers. *J. Phys. Chem. B* **2006**, *110*, 1959–1963.

(17) García-Santamaría, F.; Brovelli, S.; Viswanatha, R.; Hollingsworth, J. A.; Htoon, H.; Crooker, S. A.; Klimov, V. I. Breakdown of Volume Scaling in Auger Recombination in CdSe/CdS Heteronanocrystals: The Role of the Core–Shell Interface. *Nano Lett.* **2011**, *11*, 687–693.

(18) Klimov, V. I.; Mikhailovsky, A. A.; Xu, S.; Malko, A.; Hollingsworth, J. A.; Leatherdale, C. A.; Eisler, H. J.; Bawendi, M. G. Optical Gain and Stimulated Emission in Nanocrystal Quantum Dots. *Science* **2000**, *290*, 314–317.

(19) Zhang, C.; Xu, J.; Zhu, T.; Zhang, F.; Tan, Z.; Schiff, S. J.; Su, H.; Gao, S.; Wang, A. Y. Quantum Efficiency of Stimulated Emission in Colloidal Semiconductor Nanocrystal Quantum Dots. *Phys. Rev. B* **2009**, *80*, 035333.

(20) Irvine, S. E.; Staudt, T.; Rittweger, E.; Engelhardt, J.; Hell, S. W. Direct Light-Driven Modulation of Luminescence from Mn-Doped ZnSe Quantum Dots. *Angew. Chem., Int. Ed.* **2008**, *47*, 2685–2688.

(21) He, Y.; Wang, H.-F.; Yan, X.-P. Exploring Mn-Doped ZnS Quantum Dots for the Room-Temperature Phosphorescence Detection of Enoxacin in Biological Fluids. *Anal. Chem.* **2008**, *80*, 3832–3837.

(22) Chen, Y.; Vela, J.; Htoon, H.; Casson, J. L.; Werder, D. J.; Bussian, D. A.; Klimov, V. I.; Hollingsworth, J. A. Giant" Multishell CdSe Nanocrystal Quantum Dots with Suppressed Blinking. *J. Am. Chem. Soc.* **2008**, *130*, 5026–5027.

(23) García-Santamaría, F.; Chen, Y.; Vela, J.; Schaller, R. D.; Hollingsworth, J. A.; Klimov, V. I. Suppressed Auger Recombination in

"Giant" Nanocrystals Boosts Optical Gain Performance. *Nano Lett.* **2009**, *9*, 3482−3488.
(24) Vela, J.; Htoon, H.; Chen, Y.; Park, Y.-S.; Ghosh, Y.; Goodwin, P. M.; Werner, J. H.; Wells, N. P.; Casson, J. L.; Hollingsworth, J. A. Effect of Shell Thickness and Composition on Blinking Suppression and the Blinking Mechanism in 'Giant' CdSe/CdS Nanocrystal Quantum Dots. *J. Biophotonics* **2010**, *3*, 706−717.
(25) Spinicelli, P.; Buil, S.; Quélin, X.; Mahler, B.; Dubertret, B.; Hermier, J. P. Bright and Grey States in CdSe-CdS Nanocrystals Exhibiting Strongly Reduced Blinking. *Phys. Rev. Lett.* **2009**, *102*, 136801.
(26) Htoon, H.; Malko, A. V.; Bussian, D.; Vela, J.; Chen, Y.; Hollingsworth, J. A.; Klimov, V. I. Highly Emissive Multiexcitons in Steady-State Photoluminescence of Individual "Giant" CdSe/CdS Core/Shell Nanocrystals. *Nano Lett.* **2010**, *10*, 2401−2407.
(27) Guo, Y.; Marchuk, K.; Sampat, S.; Abraham, R.; Fang, N.; Malko, A. V.; Vela, J. Unique Challenges Accompany Thick-Shell CdSe/nCdS (n > 10) Nanocrystal Synthesis. *J. Phys. Chem. C* **2012**, *116*, 2791−2800.
(28) Bussian, D. A.; Malko, A. V.; Htoon, H.; Chen, Y.; Hollingsworth, J. A.; Klimov, V. I. Quantum Optics with Nanocrystal Quantum Dots in Solution: Quantitative Study of Clustering. *J. Phys. Chem. C* **2009**, *113*, 2241−2246.
(29) Lesoine, M. D.; Bose, S.; Petrich, J. W.; Smith, E. A. Supercontinuum Stimulated Emission Depletion Fluorescence Lifetime Imaging. *J. Phys. Chem. B* **2012**, *116*, 7821−7826.
(30) Marchuk, K.; Guo, Y.; Sun, W.; Vela, J.; Fang, N. High-Precision Tracking with Non-Blinking Quantum Dots Resolves Nanoscale Vertical Displacement. *J. Am. Chem. Soc.* **2012**, *134*, 6108−6111.
(31) Fitzpatrick, J. A. J.; Yan, Q.; Sieber, J. J.; Dyba, M.; Schwarz, U.; Szent-Gyorgyi, C.; Woolford, C. A.; Berget, P. B.; Waggoner, A. S.; Bruchez, M. P. STED Nanoscopy in Living Cells Using Fluorogen Activating Proteins. *Bioconjugate Chem.* **2009**, *20*, 1843−1847.